

## Electronic Supplementary Information

### **Ru(II)/BODIPY core co-encapsulated ratiometric nanotools for intracellular O<sub>2</sub> sensing in live cancer cells.**

Karmel Sofia Gkika<sup>a</sup>, Anna Kargaard<sup>c</sup>, Christopher S. Burke<sup>a,c</sup>, Ciaran Dolan<sup>a</sup>, Andreas Heise<sup>b,c,d</sup> and Tia E. Keyes<sup>\*a</sup>

<sup>a</sup>School of Chemical Sciences, National Centre for Sensor Research, Dublin City University, Glasnevin, Dublin 9, Ireland. E-mail: [tia.keyes@dcu.ie](mailto:tia.keyes@dcu.ie)

<sup>b</sup>CÚRAM, SFI Research Centre for Medical Devices

<sup>c</sup>Department of Chemistry, RCSI, Dublin, Ireland

<sup>d</sup>AMBER, The SFI Advanced Materials and Bioengineering Research Centre

# Contents

Materials and Methods .....	3
Synthesis of ruthenium intermediate compounds .....	3
<b>Preparation of [Ru(dpp)(DMSO)<sub>2</sub>Cl<sub>2</sub>] (2)</b> .....	3
<b>Preparation of [Ru(dpp)(phen-NH<sub>2</sub>) (ox)] (3)</b> .....	3
Synthesis and Characterization .....	4
NMR and Mass Spectrometry Analysis .....	4
RuBDP NPs: SEM and DLS Characterization .....	11
Photophysical Characterisation of RuBDP components and nanoparticles .....	12
Cell Studies .....	17
References .....	28

## Materials and Methods

### Synthesis of ruthenium intermediate compounds

#### Preparation of [Ru(dpp)(DMSO)<sub>2</sub>Cl<sub>2</sub>] (**2**)

cis, fac-[Ru(DMSO)<sub>4</sub>Cl<sub>2</sub>] (408.7 mg, 0.844 mmol) and dpp (0.844 mmol) were heated at reflux in ethanol (30 mL) for 3 h where the solution progressed from a yellow/brown to an orange/ brown solution. The mixture was cooled to RT and was then concentrated in vacuo, filtered and washed with minimal cold ethanol. The light-orange solids were washed with diethyl ether and dried under vacuum. Yield: 296.2 mg (56 %). <sup>1</sup>H NMR (600 MHz, CDCl<sub>3</sub>) δ (ppm): 10.16 (d, 1H); 9.96 (d, 1H); 8.01 (q, 2H); 7.88 (d, 1H); 7.72 (d, 1H); 7.62 – 7.56 (m, 8H), 7.53 (d, 1H), 7.52 (d, 1H), 3.67 (s, 3H); 3.61 (s, 3H); 3.26 (s, 3H); 2.69 (s, 3H).

#### Preparation of [Ru(dpp)(phen-NH<sub>2</sub>) (ox)] (**3**)

[Ru(dpp)(phen)(DMSO)<sub>2</sub>Cl<sub>2</sub>] (680 mg, 1.096 mmol) and sodium oxalate (1.6 mmol) were heated at reflux in water (10 mL) for 90 min (orange solution). The reaction was cooled to RT. A hot solution of phen-NH<sub>2</sub> (1.096 mmol) in Ethylene Glycol (5 mL) was added to the reaction and was refluxed for 3 ½ h. The dark brown/purple mixture was cooled to RT and was added dropwise to stirring water (20 mL). After 30 min the dark purple precipitate formed was filtered through a 0.45 μm membrane and was washed with water (15 mL) and minimal acetone and dried overnight under vacuum. Yield isomer mixture: 620.3 mg (79 %). <sup>1</sup>H NMR (600 MHz, DMSO-d<sub>6</sub>) δ (ppm): 9.81 (dd, 2H); 9.69 (d, 1H); 9.38 (d, 1H), 8.64 (dd, 1H), 8.63-8.62 (2H), 8.51 (d, 1 H), 8.43-8.36 (m, 2H), 8.24 (d, 2H); 8.09 (dd, 1 H); 8.14-8.11 (dd, 2H); 8.07-8.04 (dd, 1H); 7.93-8.01 (6H), 7.81 (d, 1H), 7.65 (q, 1H); 7.42 (2 s, 1H); 7.13 (2 s, 2H).

## Synthesis and Characterization

### NMR and Mass Spectrometry Analysis

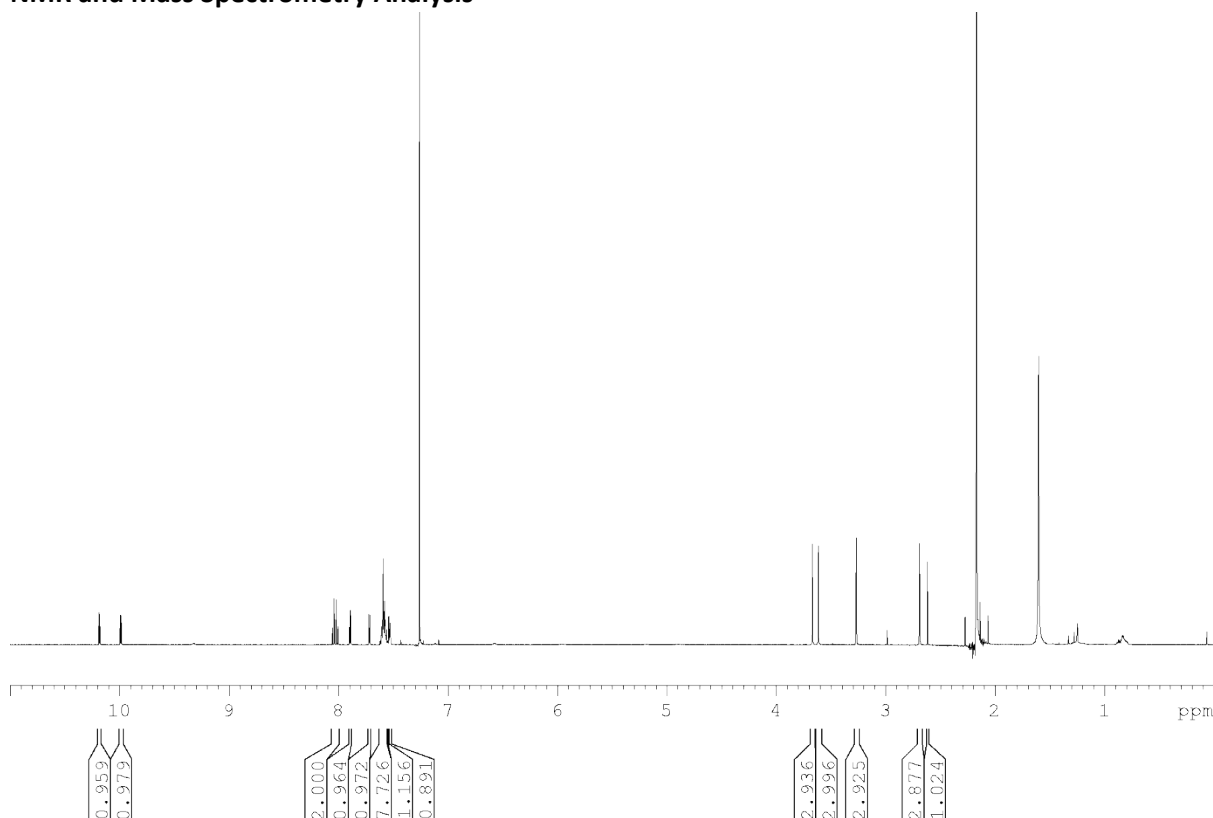


Figure S 1: <sup>1</sup>H NMR of [Ru(dpp)(DMSO)<sub>2</sub>Cl<sub>2</sub>] (**2**) in CDCl<sub>3</sub> with aromatic region of interest inset, 600 MHz.

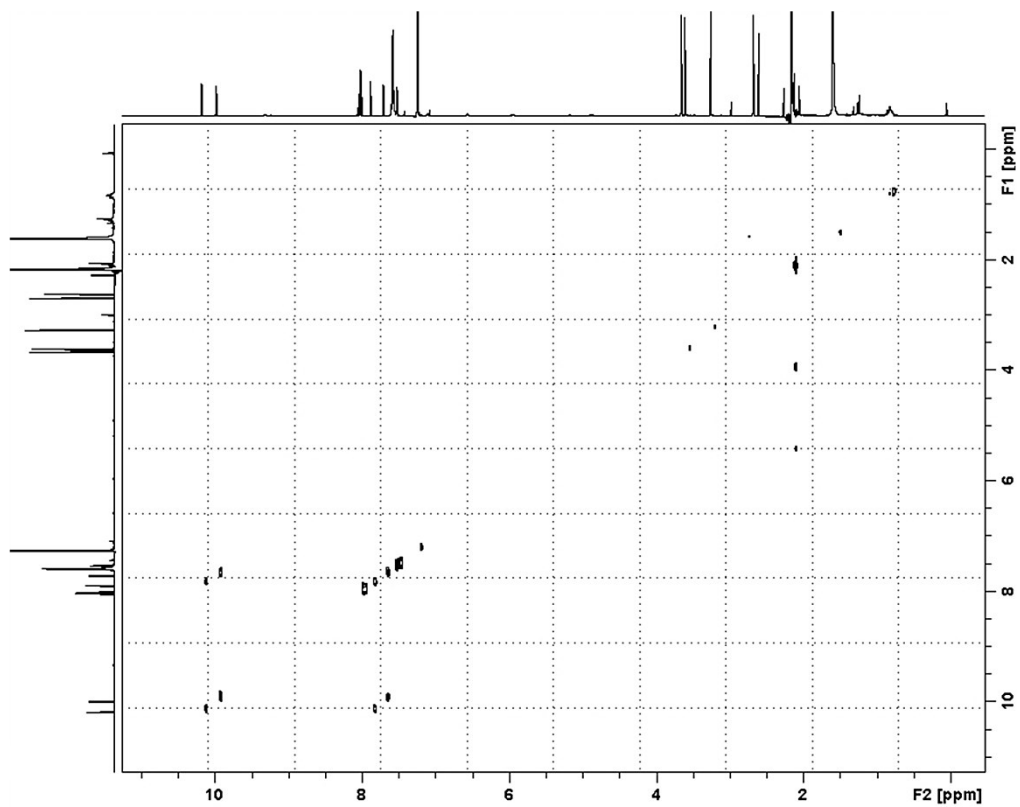


Figure S 2: COSY spectrum of **2** in  $\text{CDCl}_3$ , 600 MHz.

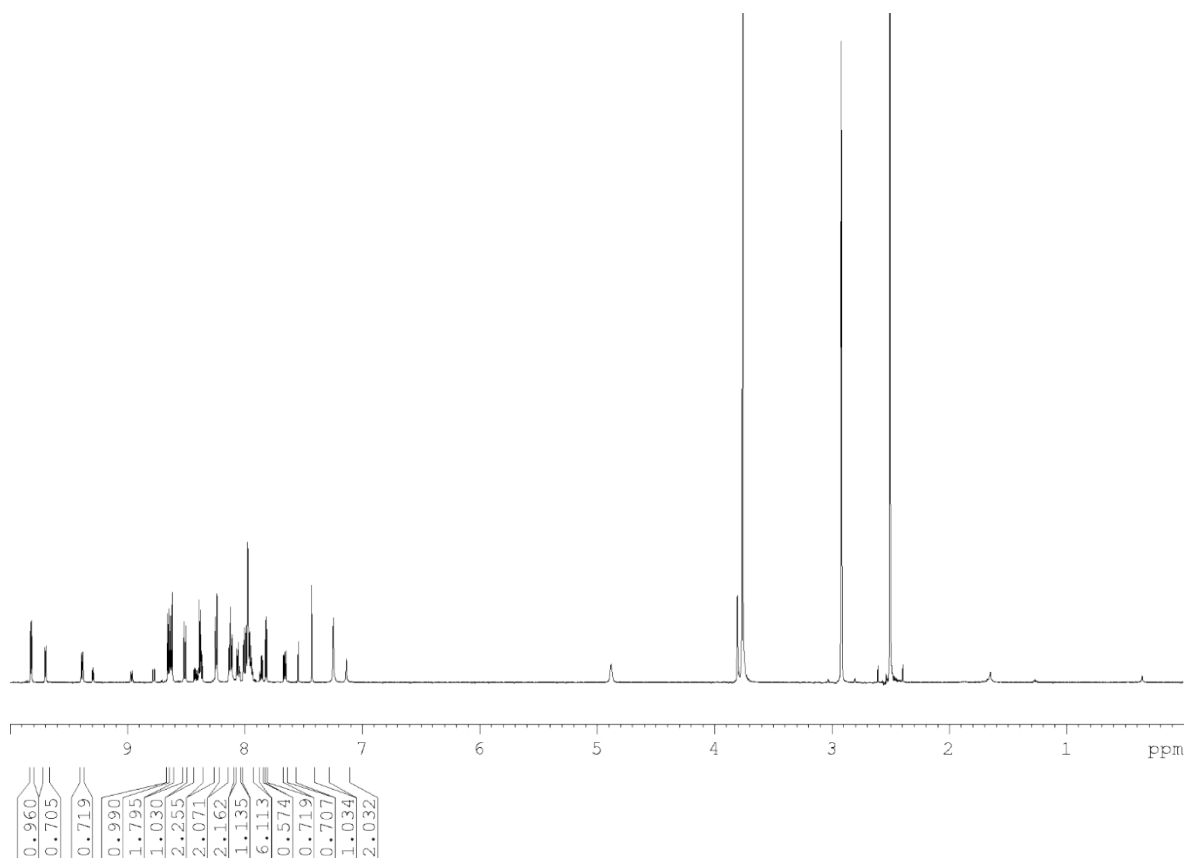


Figure S 3:  $^1\text{H}$  NMR of  $[\text{Ru}(\text{dpp})(\text{phen-NH}_2)(\text{ox})]$  (**3**) in  $\text{DMSO-d}_6$ , 600 MHz.

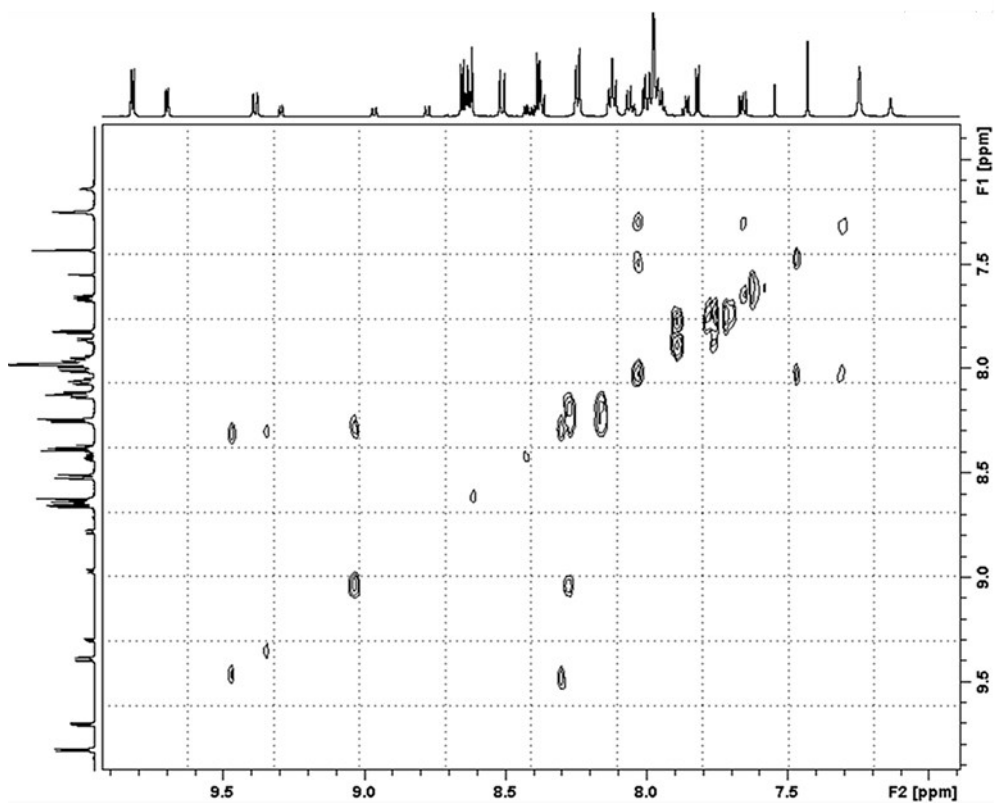


Figure S 4: COSY spectrum of **3** in DMSO- $d_6$ , 600 MHz.

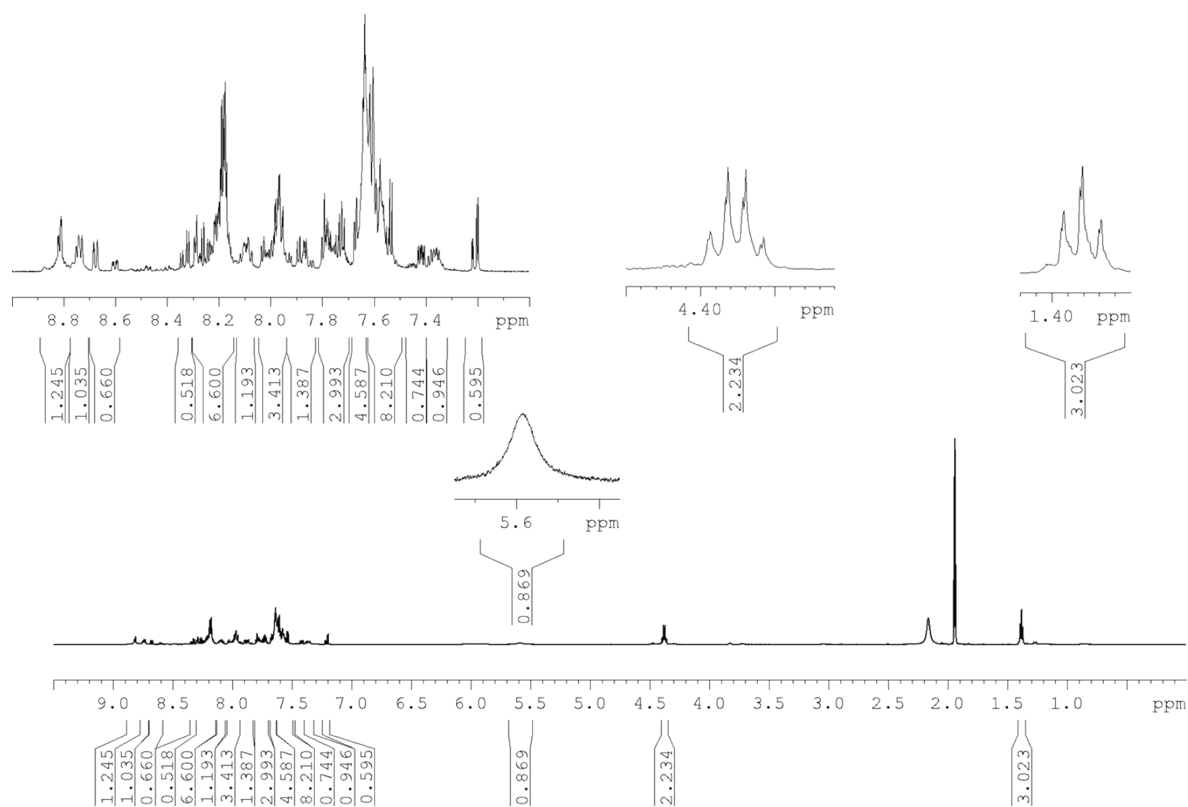


Figure S 5:  $^1\text{H}$  NMR of  $[\text{Ru}(\text{dpp})(\text{phen-NH}_2)(\text{bpybenzCOOEt})]^{2+}$  (**4**) in MeCN- $d_3$ , 400 MHz.

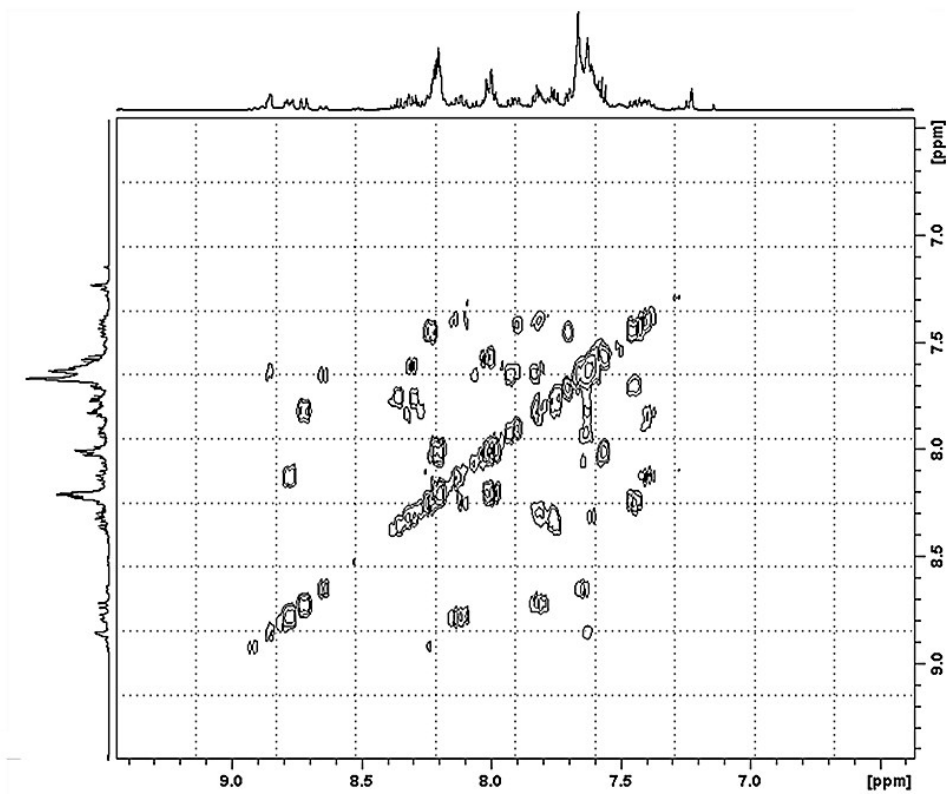
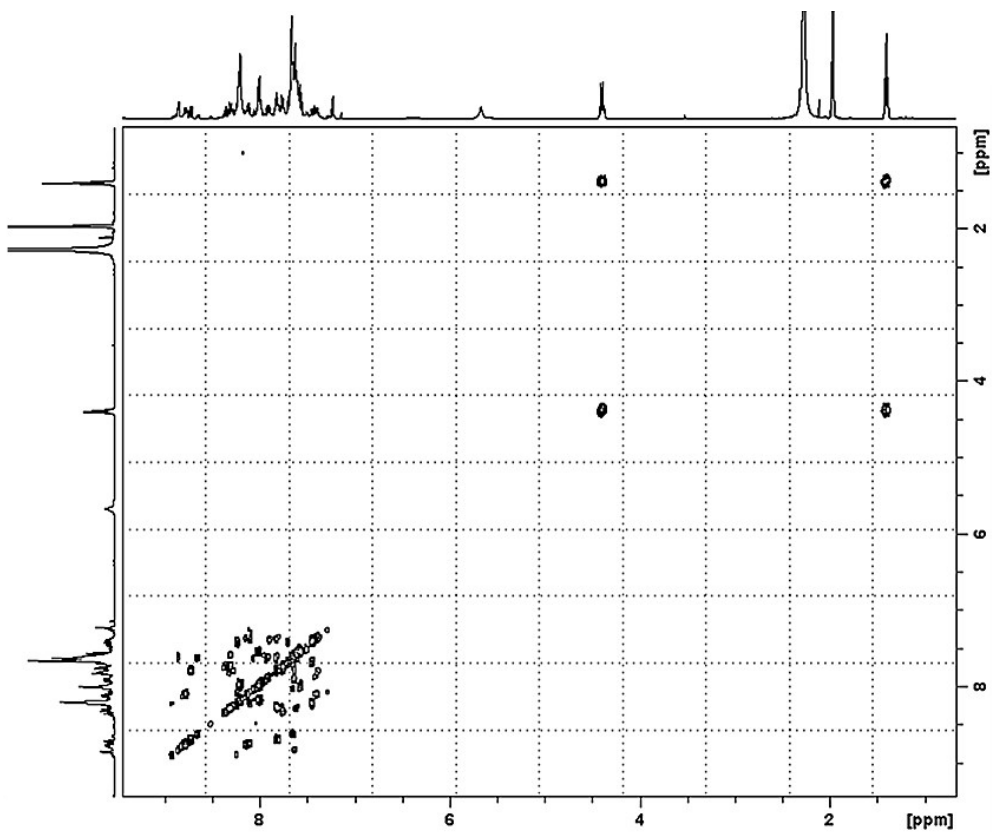


Figure S 6: Full range COSY spectrum (top) and expanded aromatic region of compound 4 MeCN-d<sub>3</sub>, 600 MHz.

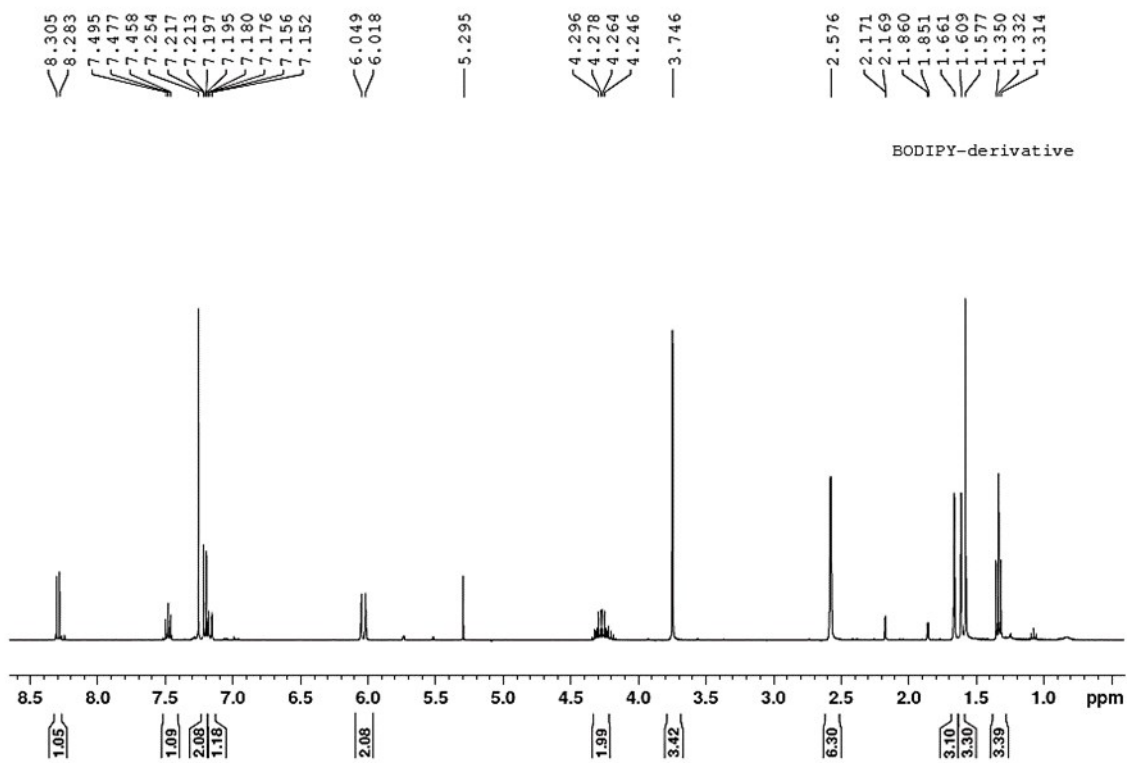


Figure S 7:  $^1\text{H}$  NMR of 2, 6 diethyl- 1, 3, 5, 7- tetramethyl- 8-(2-fluorophenyl)-6methoxy- 1, 5- naphthyridine- 4,4'- difluoroboradiazindacene (**BODIPY**) in  $\text{CDCl}_3$ , 400 MHz.

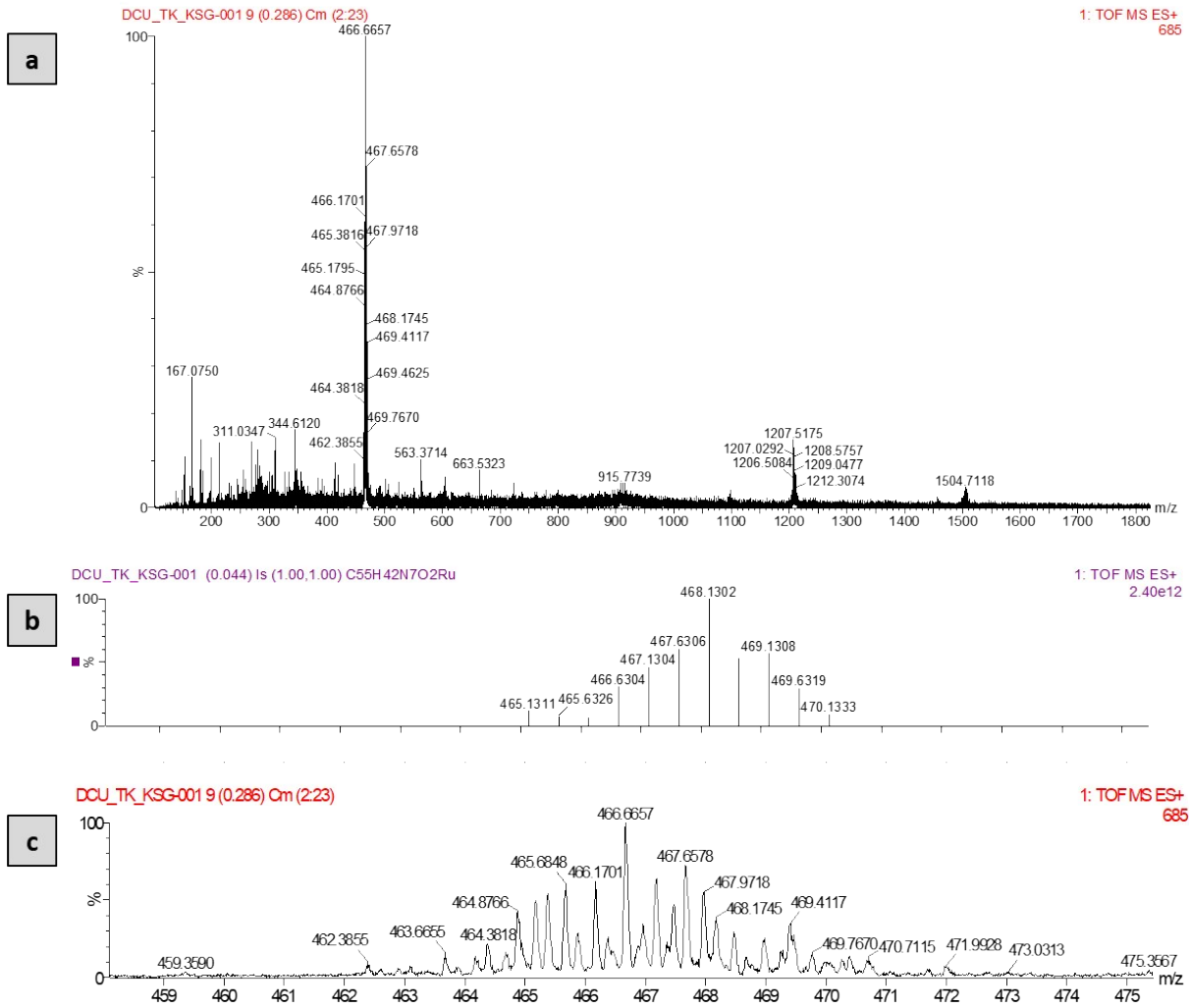


Figure S 8: HR-MS of **4** in ESI (+) mode: (a) full range, (b) expansion of the isotope model and (c) expansion of the isotope pattern obtained from the mass spectrum.



## RuBDP NPs: SEM and DLS Characterization

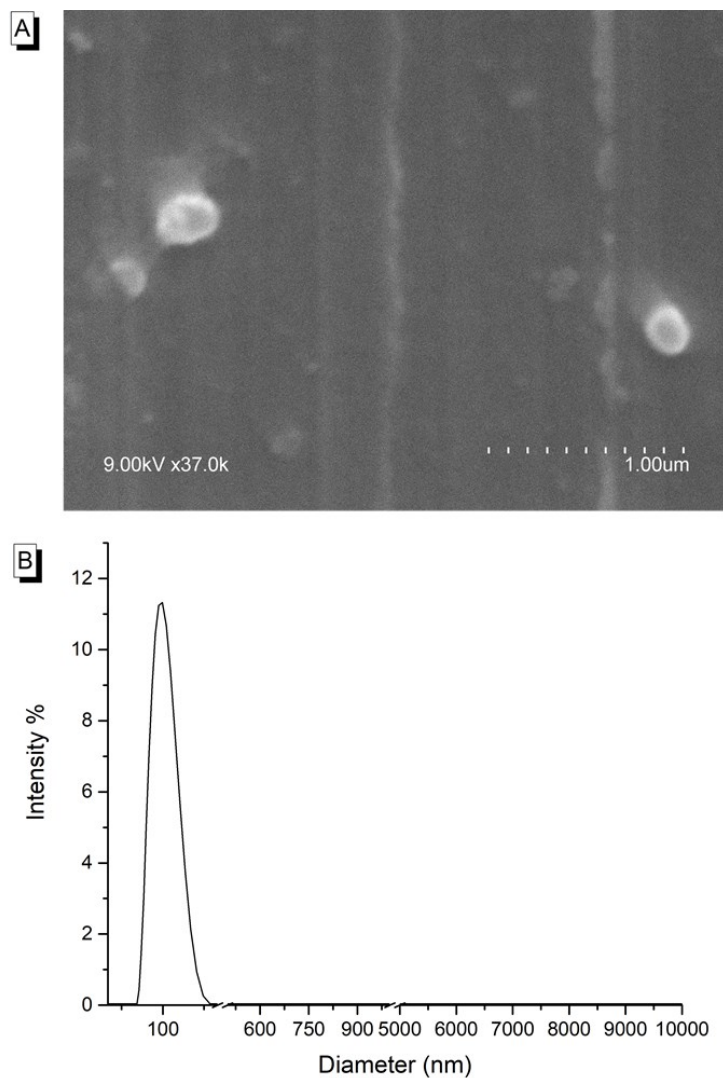


Figure S 9: (A) SEM image (9.00 kV x 37.0k) (B) DLS intensity particle size distribution; Zeta potential was measured to be  $25 \pm 1.37$  mV and conductivity of 16.8 (n=3).

## Photophysical Characterisation of RuBDP components and nanoparticles

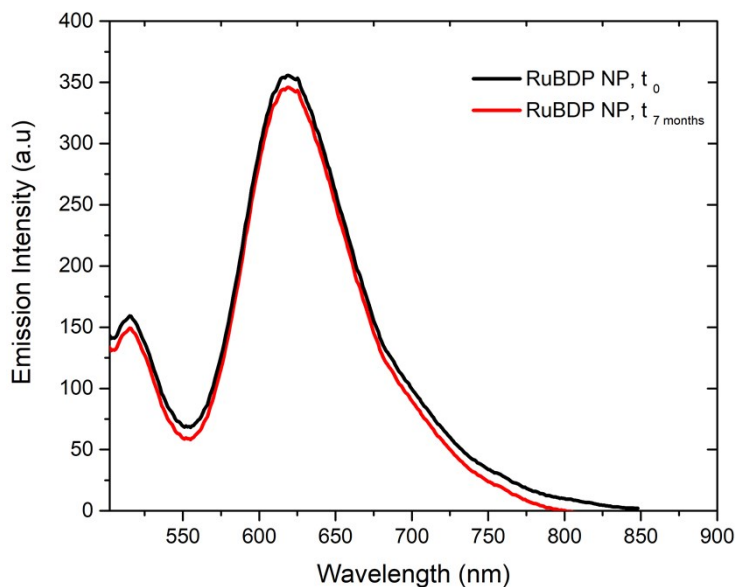


Figure S 10: Emission spectra of a new and seven- month suspension of RuBDP NPs in PBS following excitation at 480 nm; excitation and emission slit widths set at 10 nm.

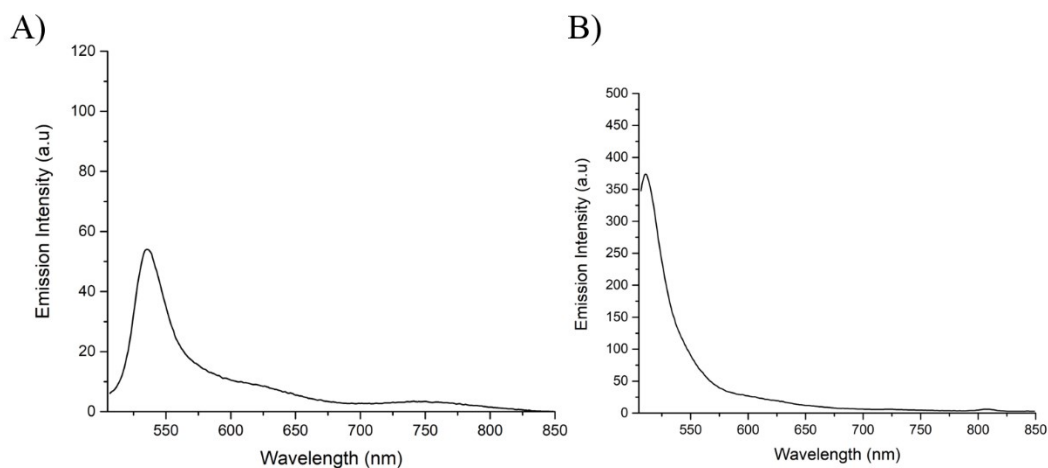


Figure S 11: Emission spectra of (A) core-shell RuBODIPY particle- (previously reported)<sup>3</sup> and (B) core co-encapsulated RuBDP NPs - supernatant collected following swelling with THF.

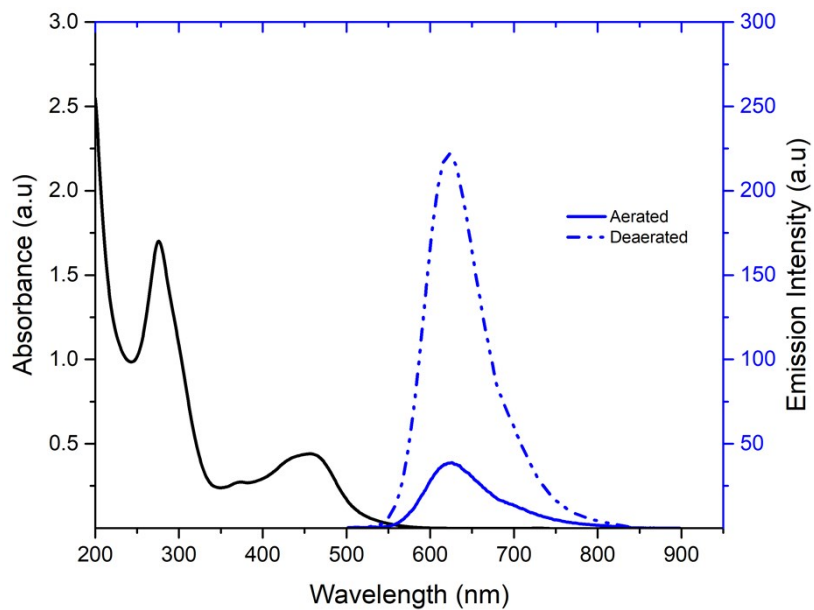
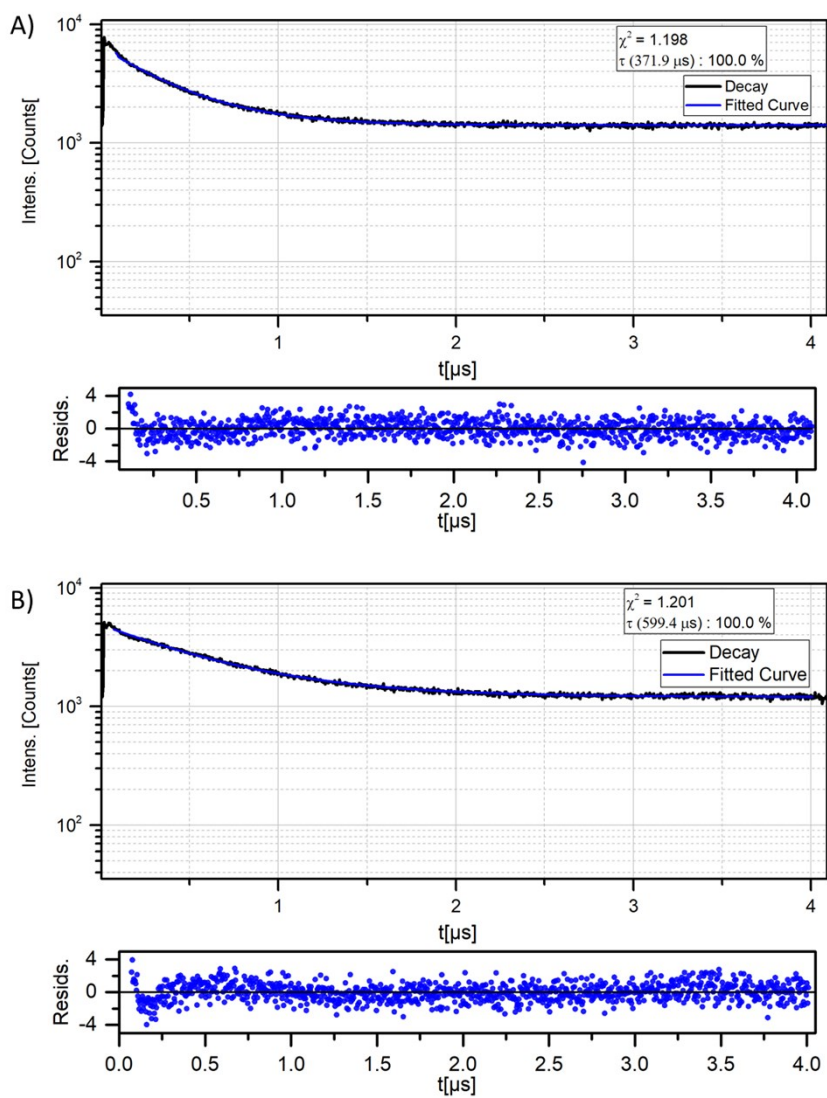


Figure S 12: Absorbance and emission spectra of  $[\text{Ru}(\text{dpp})(\text{phen-NH}_2)(\text{bpy-benz-COOEt})]^{2+}$  in MeCN at 15  $\mu\text{M}$ . Emission spectra were recorded under aerated and deaerated conditions following excitation at 460 nm; excitation and emission slit widths set at 5 nm.



$$\int_{-\infty}^t IRF(t') \sum_{i=1}^x A_i e^{-\frac{t-t'}{\tau_i}} dt'$$

Figure S 13: Emission Decays of parent complex  $[\text{Ru}(\text{dpp})(\text{phen-NH}_2)(\text{bpyArCOOEt})]^{2+}$  in aerated and deaerated acetonitrile (15  $\mu\text{M}$ ); Residual plots for the exponential fitting of both curves are shown below each plot.

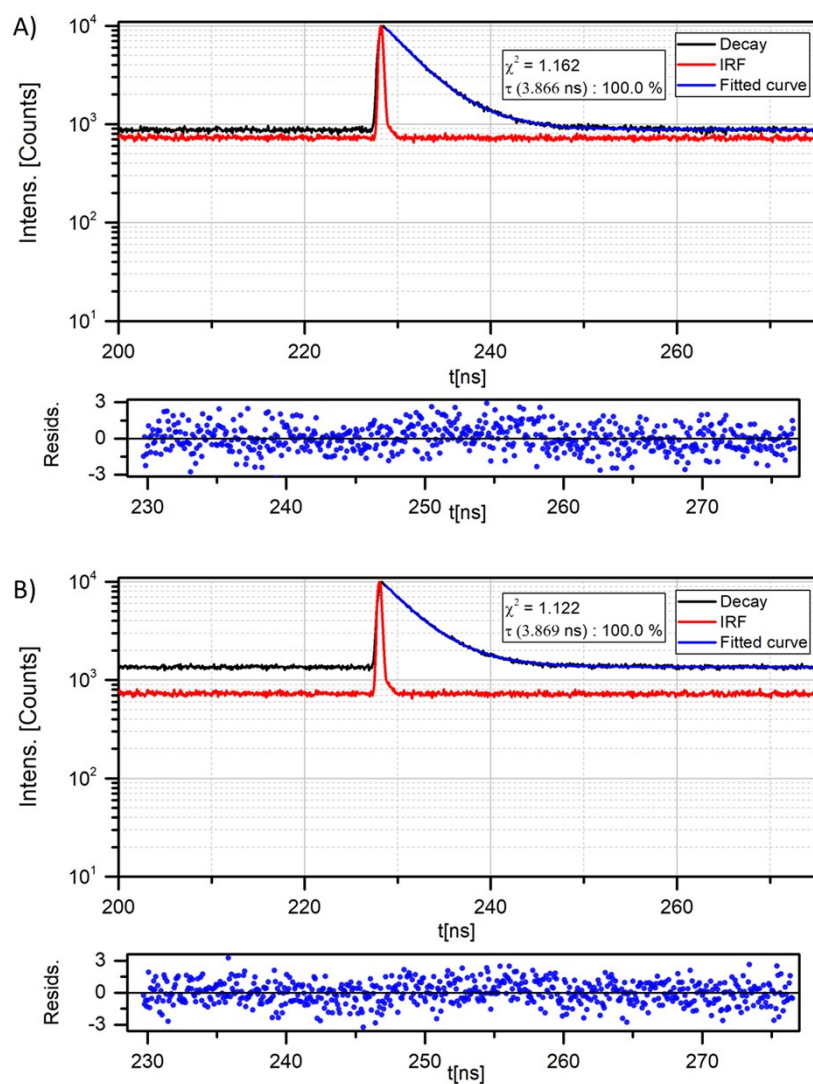
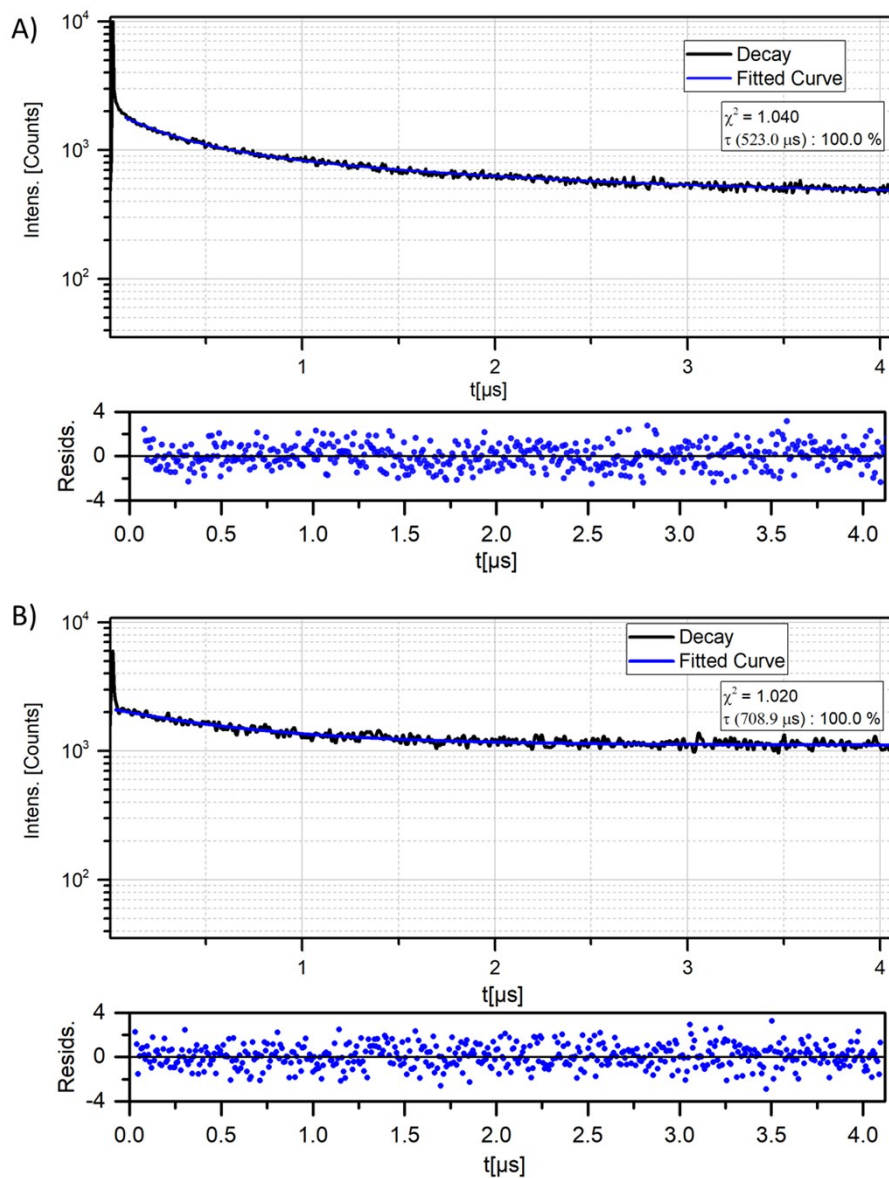


Figure S 14: Emission Decays of the BODIPY reference core component under (A) aerated and (B) deaerated conditions of RuBDP NPs in PBS (pH 7.4); Residual plots for the exponential fitting of both curves are shown below each plot.

$$\int_{-\infty}^t IRF(t') \sum_{i=1}^x A_i e^{-\frac{t-t'}{t_1}} dt'$$



$$\int_{-\infty}^t IRF(t') \sum_{i=1}^x A_i e^{-\frac{t-t'}{\tau_i}} dt'$$

Figure S 15: Emission Decays of the Ru(II) O<sub>2</sub> sensor core component under (A) aerated and (B) deaerated conditions of RuBDP NPs in PBS (pH 7.4); Residual plots for the exponential fitting of both curves are shown below each plot.

## Cell Studies

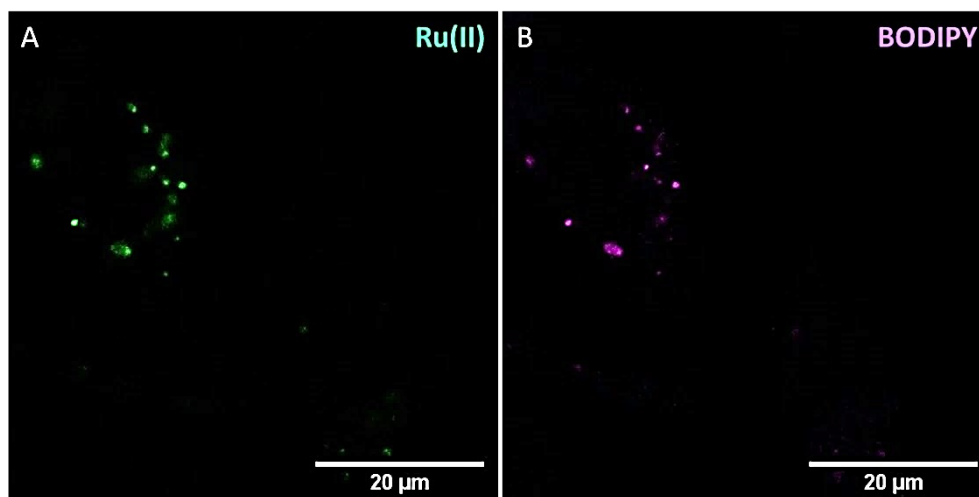


Figure S 16: HeLa cells were treated with RuBDP NPs ( $4.5 \mu\text{g mL}^{-1}$ ), incubated for 4 h at  $37^\circ\text{C}$  and excited using 480 nm white light laser. (A) Emission collected within 569 – 850 nm corresponding to the  $[\text{Ru}(\text{dpp})(\text{phen-NH}_2)(\text{bpybenzCOOEt})]^{2+}$  component and (B) Emission collected within 505 – 550 nm corresponding to the BODIPY dye.

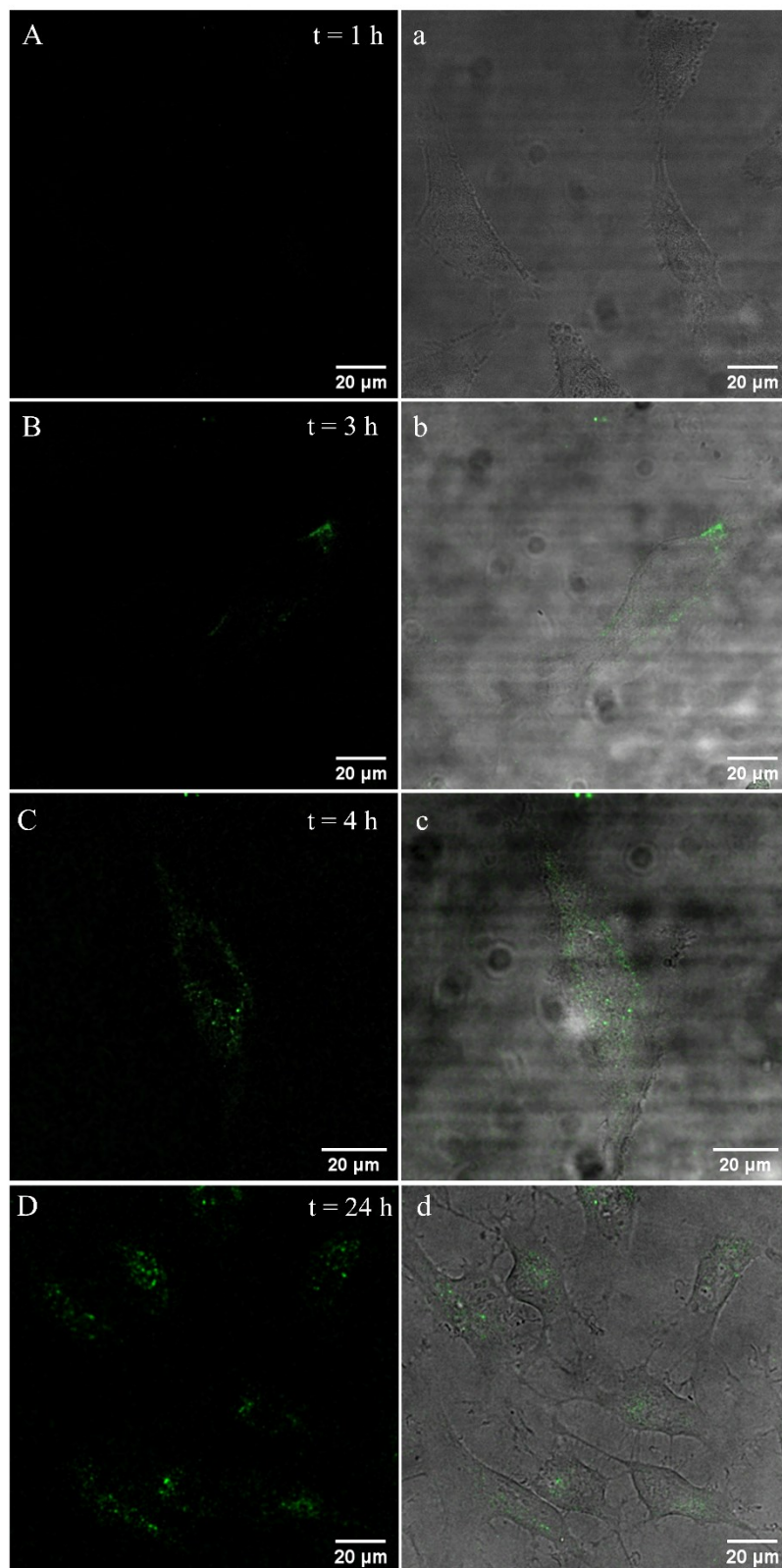


Figure S 17: Confocal luminescence images of RuBDP NPs in live HeLa cells where the Ru(II) emission channel and overlay are shown. Cells were incubated in the absence of light with  $4.5 \mu\text{g mL}^{-1}$  nanoparticles over 24 h. RuBDP NPs were excited using 480 nm white light laser and the emission was collected between 569 nm and 800 nm for the Ru(II) channel.



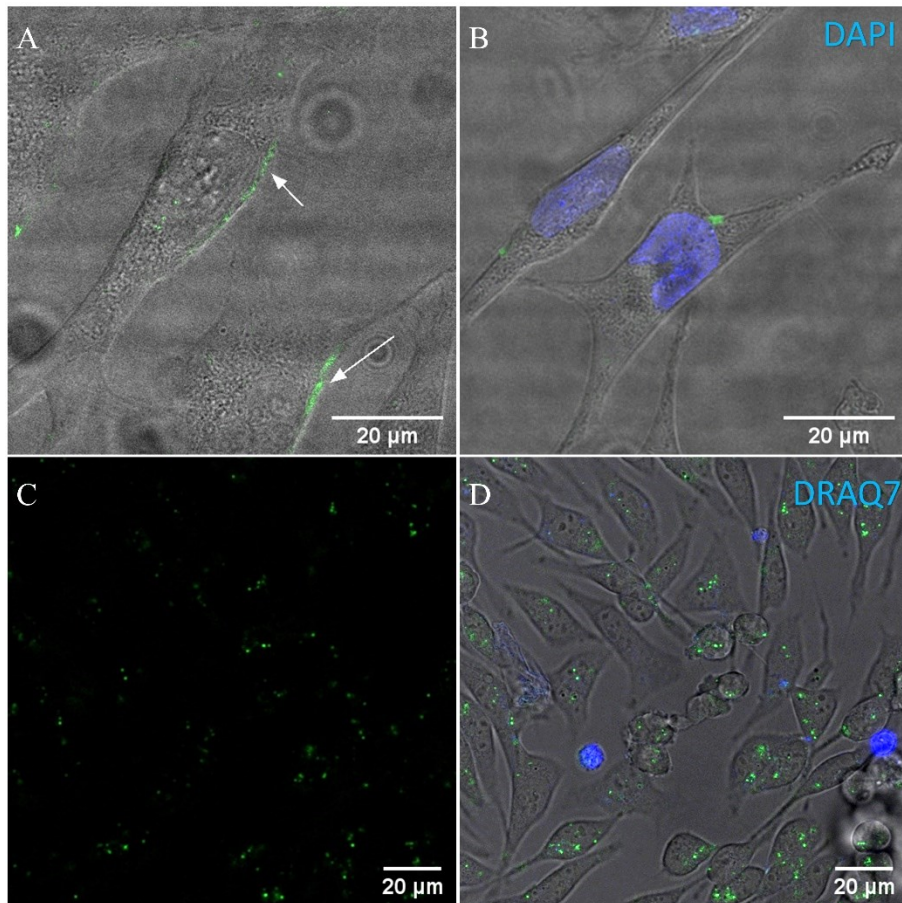


Figure S 18: Uptake of RuBDP NPs in live CHO cells at variant concentrations and incubation periods. (A) Absence of NP internalization at  $4.5 \mu\text{g mL}^{-1}$ / 4 h incubation, (B) co-staining with DAPI probe ( $3 \mu\text{M}$ ), (C) Formation of NP aggregates at  $12 \mu\text{g mL}^{-1}$ / 24 h and (D) Cell debris and co-staining with DRAQ 7 ( $3 \mu\text{M}$ ) revealed compromised cells. The 633 nm laser was used to excite DRAQ 7 and emission was collected between 635 – 900 nm.

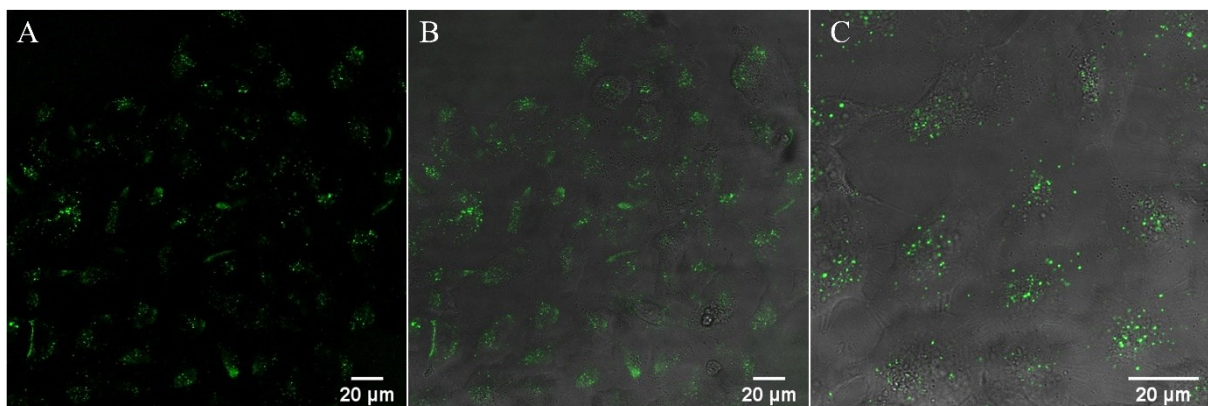


Figure S 19: Confocal luminescence imaging of RuBDP NPs in live A549 cells showing efficient uptake of particles under the same conditions of  $4.5 \mu\text{g mL}^{-1}$  / 4 h in the absence of light at  $37^\circ\text{C}$  time (63 X oil immersion objective lens). (A) RuBDP NPs were excited using the 480 nm white light laser and the emission was collected between 569 nm and 800 nm for the Ru(II) channel. (B) Overlay with brightfield and (C) Overlay

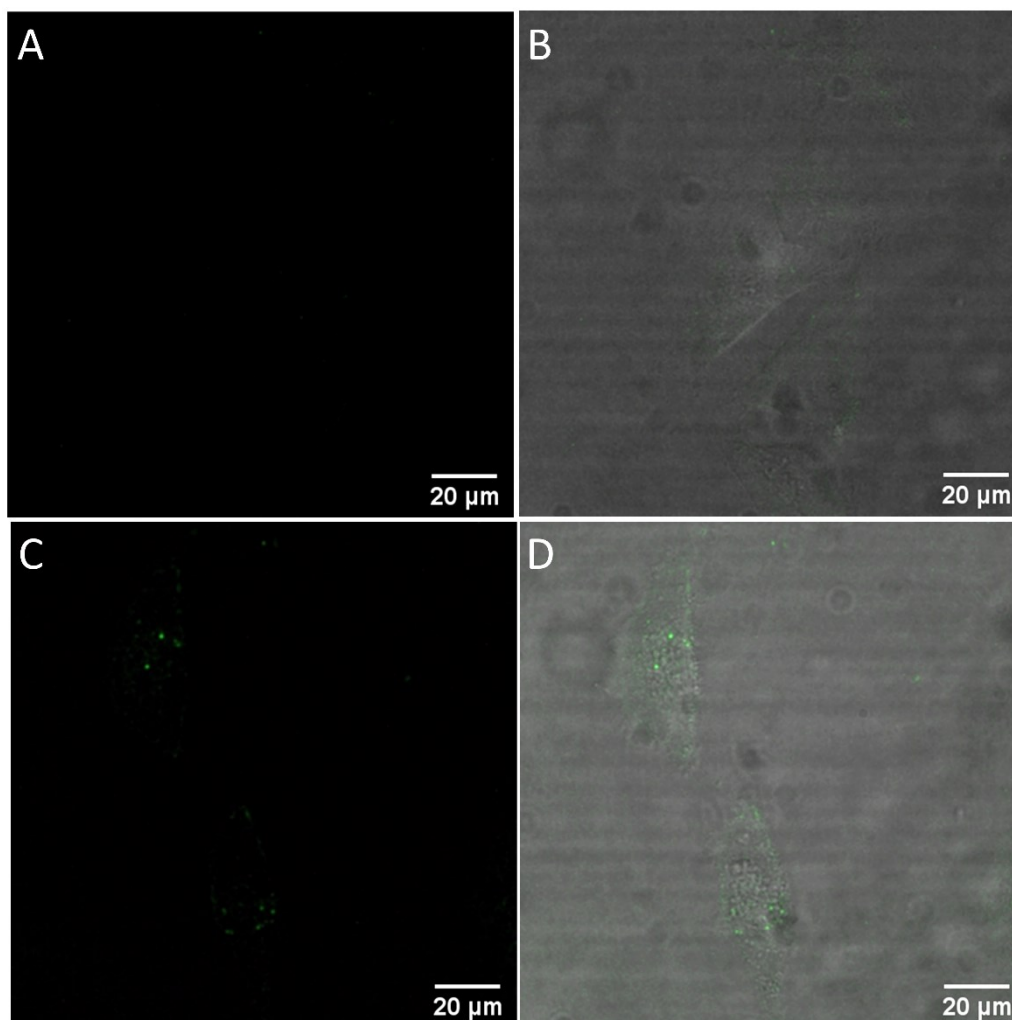


Figure S 20: HeLa cells were treated with RuBDP NPs ( $4.5 \mu\text{g mL}^{-1}$ ) and incubated for 4 h at  $4^\circ\text{C}$  time (63 X oil immersion objective lens). Confocal imaging of RuBDP NPs (A) Through-out the cells (C) At the cell surface (B-D) Overlay images with brightfield. NPs were excited using the 480 nm white light laser and emission was collected between 569 - 800 nm.

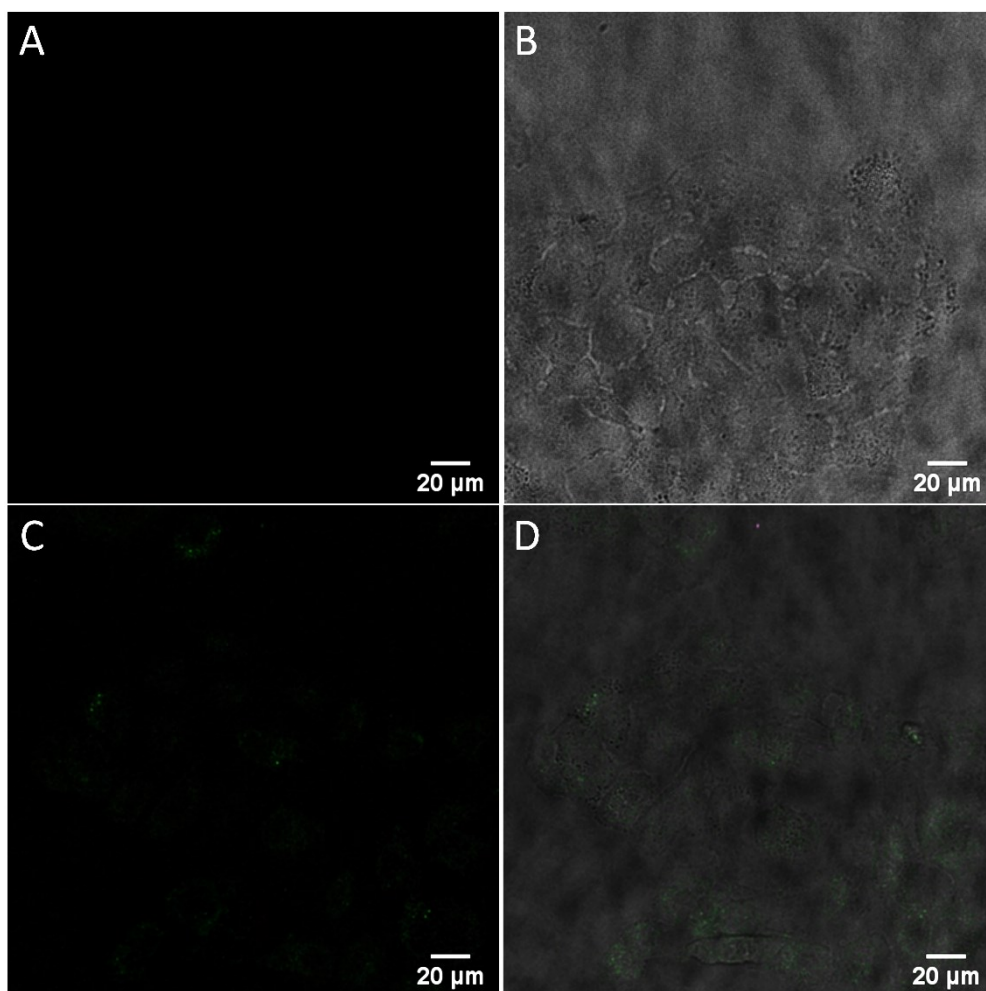


Figure S 21: Uptake of RuBDP NPs ( $4.5 \mu\text{g mL}^{-1}$ ) in A549 cells following incubation of 4 h at  $4^\circ\text{C}$  time (63 X oil immersion objective lens). Confocal imaging of RuBDP NPs (A) Through-out the cells (C) At the cell surface (B-D) Overlay images with brightfield. NPs were excited using the 480 nm white light laser and emission was collected between 569 - 800 nm.

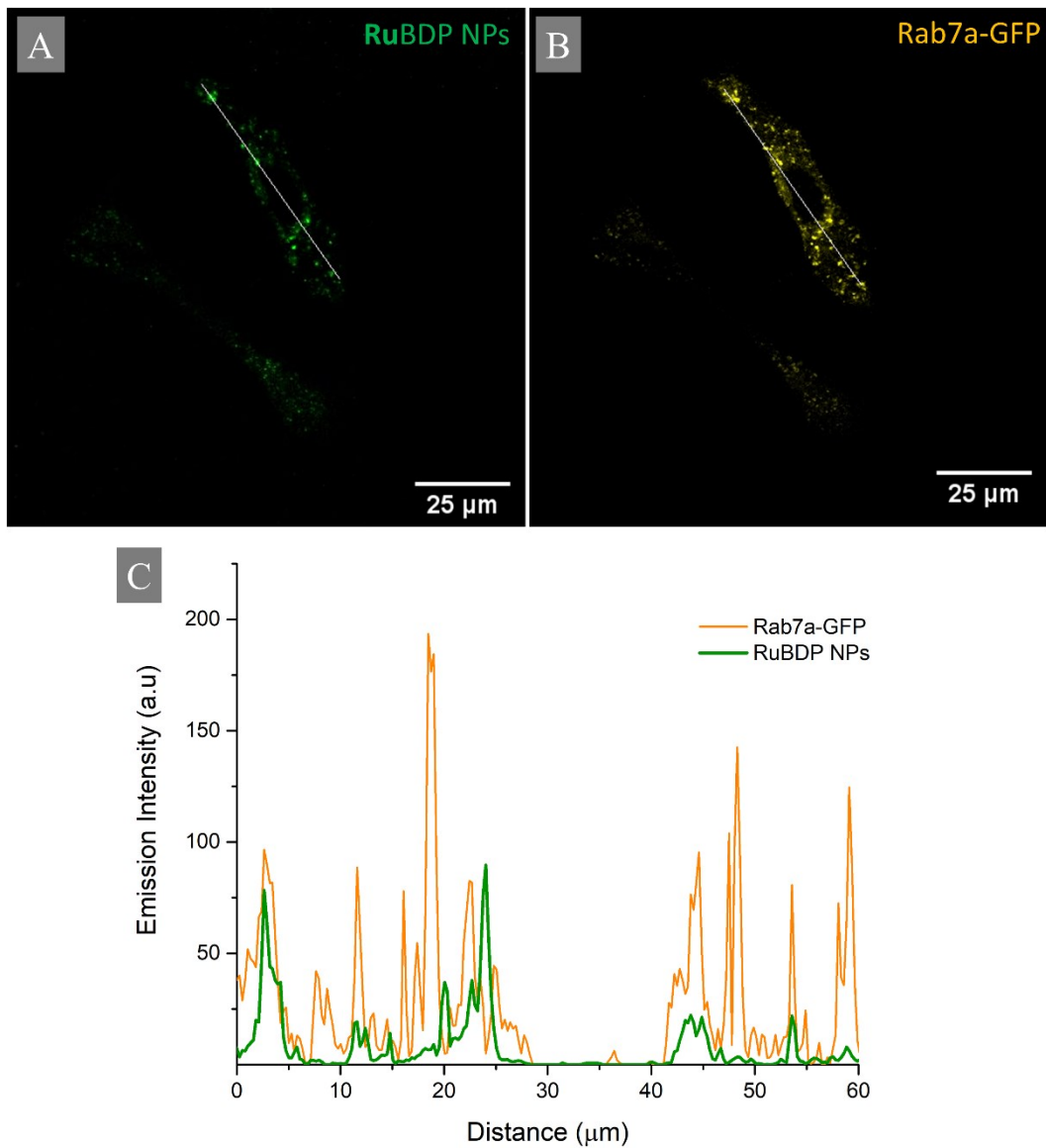


Figure S 22: Co-localization study of RuBDP NPs with Late endosomal staining probe in live A549 cells. (A) Confocal image of Ru(II)- particle component (green) (B) Rab7a-GFP (yellow) and (C) The fluorescence intensity profile of RuBDP NPs and Rab7a-GFP showing strong co-localization between the particles and the late-endosome staining dye. (ImageJ)

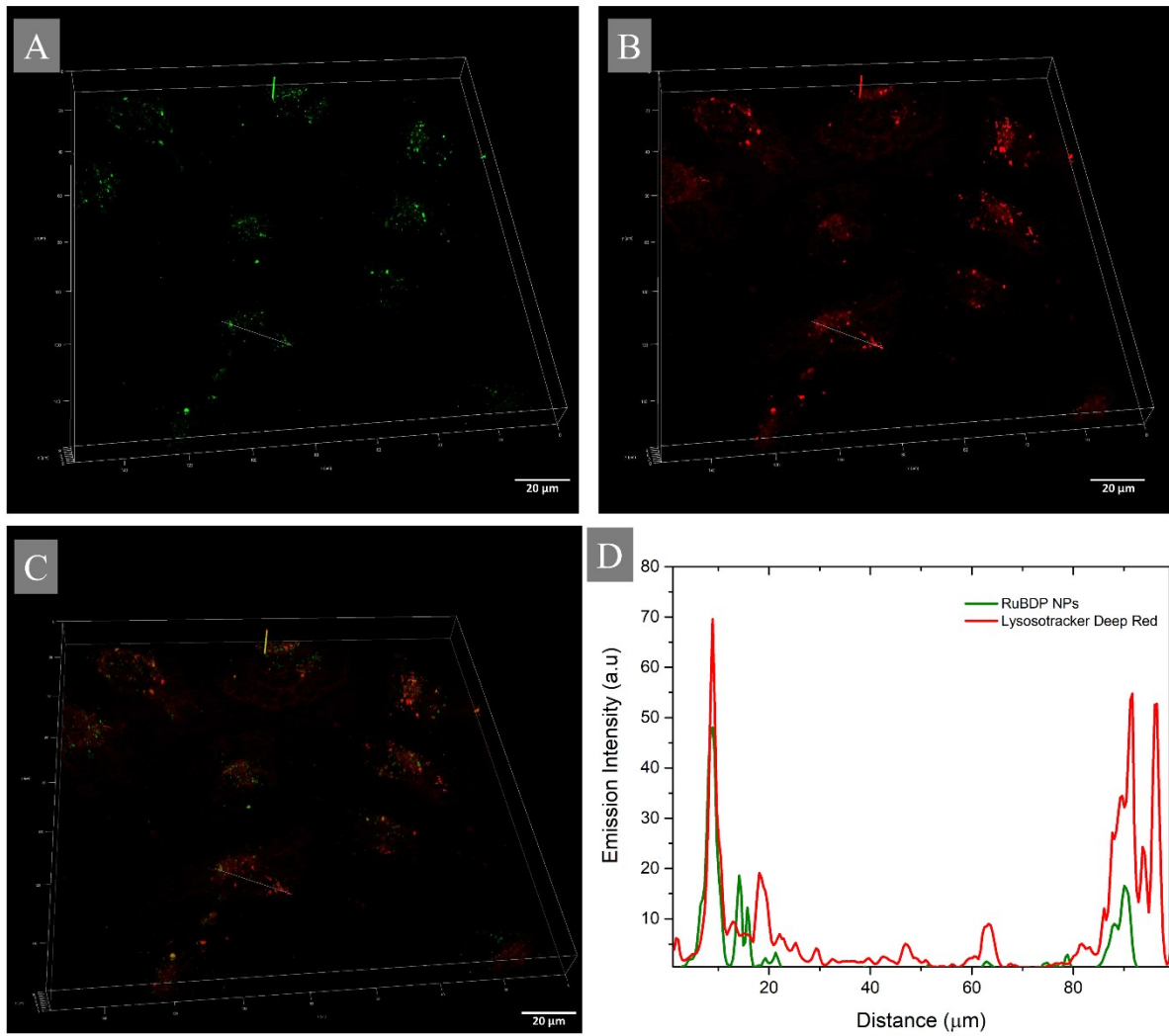


Figure S 23: Z-stack derived 3D Confocal Images of co-localization of RuBDP NPs with lysosomal staining probe in live HeLa cells where: (A) RuBDP NPs (green), (B) LysoTracker Deep Red (red;  $\lambda_{\text{exc}}$  647 nm,  $\lambda_{\text{em}}$  range: 650 – 800 nm), (C) Merged image, (D) The fluorescence intensity profiles obtained revealing partial co-localization of RuBDP NPs with LysoTracker Deep Red (ImageJ).

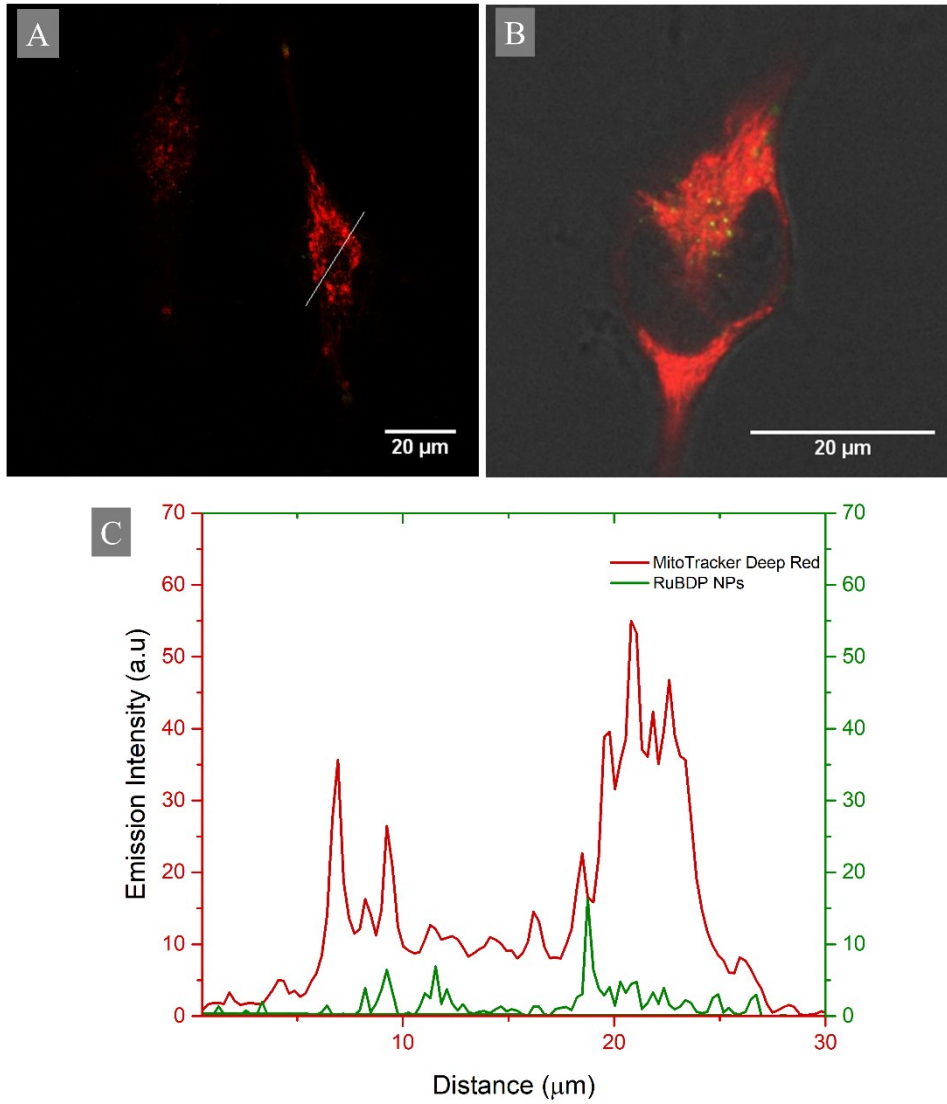


Figure S 24: Co-localization of RuBDP NPs with MitoTracker Deep Red in live HeLa cells. (A-B) RuBDP (green) and MitoTracker Deep Red (red) merged images. (C) The fluorescence intensity profile of RuBDP NPs and MitoTracker Deep red obtained from the line profile across the cell (ImageJ) showed poor co-localization between the particles and the mitochondria-staining dye. MitoTracker Deep Red was excited using the 644 nm white light laser and emission was collected between 650 and 800 nm.

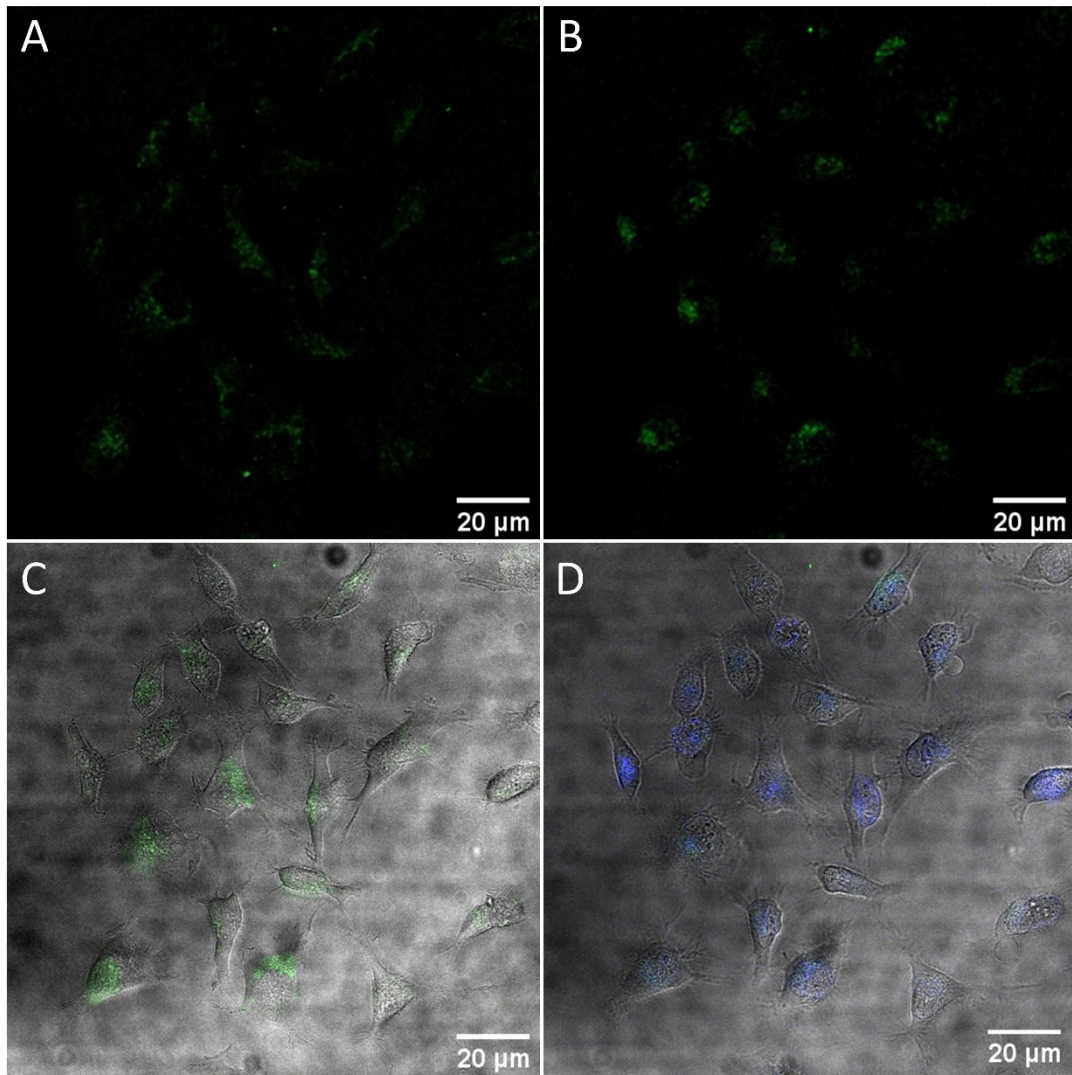


Figure S 25: Phototoxicity of RuBDP NPs in HeLa cells using excitation with 480 nm over time (63 X oil immersion objective lens). (A) Confocal imaging of NPs at  $4.5 \mu\text{g mL}^{-1}$  at the 4 h timepoint, (C) overlay and absence of DRAQ 7 confirm cell viability, (B) RuBDP NPs following 2 h of continuous irradiation, (D) overlay with DRAQ 7 (blue) internalization confirms damaged cells.

## Oxygen Mapping

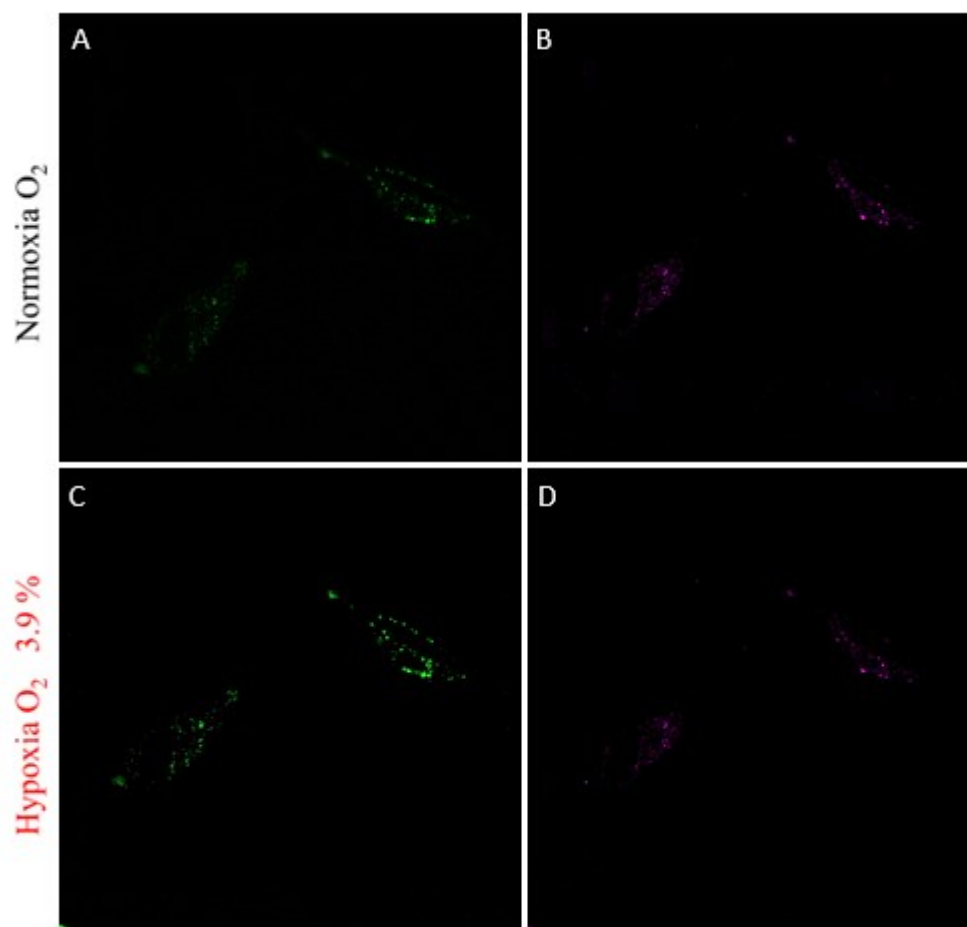


Figure S 26: Confocal imaging of HeLa cells treated with RuBDP NPs at  $4.5 \mu\text{g mL}^{-1}$  for 4 h at  $37^\circ\text{C}$ . Emission was collected corresponding to (A, C) Ru(II) O<sub>2</sub> sensitive component and (B, D) BODIPY reference probe under normoxic and hypoxic conditions.

### Plate reader-based ratiometric O<sub>2</sub> response assay



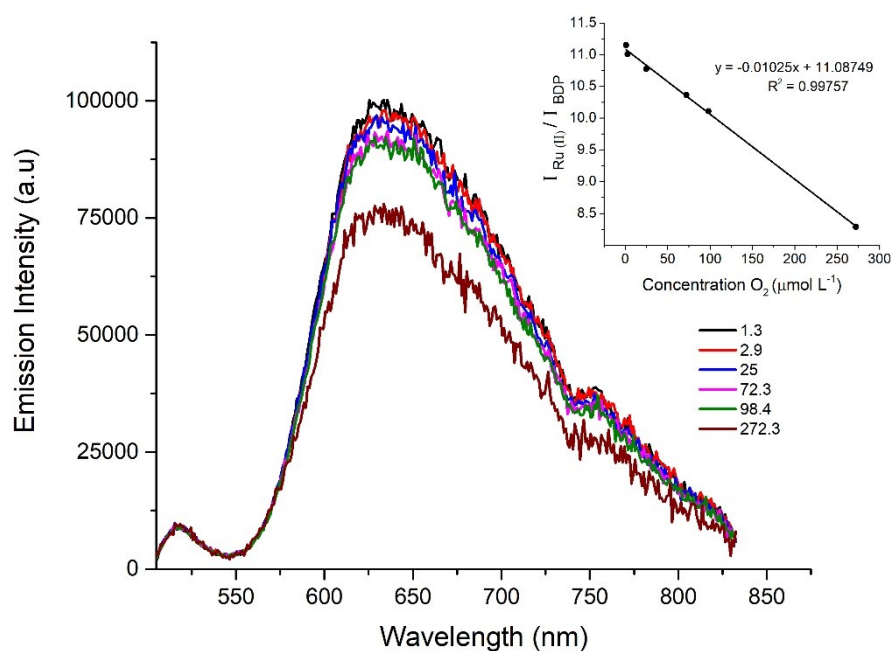


Figure S 27: Emission spectra of RuBDP NPs in PBS (pH 7.4) recorded at different concentrations of oxygen on the ClarioStar Plus plate reader. The excitation wavelength was set to 480 nm with a detection range between 505 and 840 nm. Inset: Calibration ratiometric plot of the BODIPY and Ruthenium emission intensities, at 516 nm and 632 nm respectively, as a function of oxygen concentration ( $R^2$  0.99757).

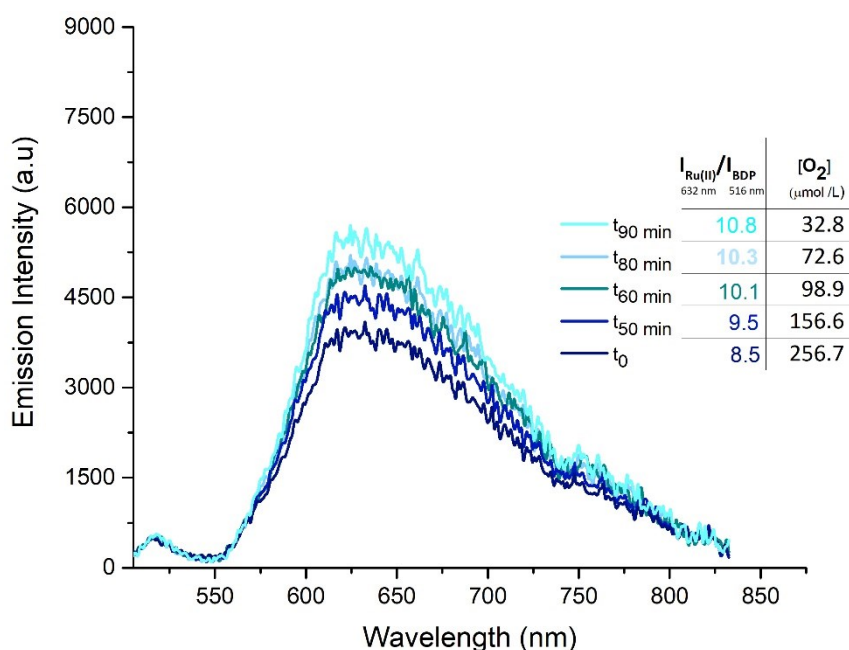


Figure S 28: RuBDP NPs ( $4.5 \mu\text{g mL}^{-1}$ ) internalized in A549 cells were excited at 480nm and emission spectra between 505 and 840 nm were collected upon treatment with sodium sulfite ( $5 \text{ mg mL}^{-1}$ ). The Stern-Volmer equation obtained from the calibration plot above was used to determine the  $[O_2]$  in cells following treatment with sodium sulfite using the ratiometric signal of  $I_{Ru(II) 632 \text{ nm}} / I_{BDP 516 \text{ nm}}$ .

## References

- 1 C. S. Burke and T. E. Keyes, *RSC Advances*, 2016, **6**, 40869–40877.
- 2 A. Martin, R. D. Moriarty, C. Long, R. J. Forster and T. E. Keyes, *Asian Journal of Organic Chemistry*, 2013, **2**, 763–778.
- 3 A. Byrne, J. Jacobs, C. S. Burke, A. Martin, A. Heise and T. E. Keyes, *Analyst*, 2017, **142**, 3400–3406.